كلية الهندسة بشبرا
FACULTY OF ENGINEERING AT SHOUBRA
ERJ
ISSN:1687-1340

ENGINEERING RESEARCH JOURNAL (ERJ)
Volume (52),Issue (1)
January 2023, pp:171-178
https://erjsh.journals.ekb.eg

# Improved PI-Controller Of Switched Reluctance Motor For Torque Ripple Minimization In Electric Vehicle Applications

**Basel Emad [1,*], Fathy El Sayed Abdel-Kader [2], M. Z. Elsherif [1] , Islam M. Abdelqawee [1]**

[1] *Electrical Engineering Department, Faculty of Engineering at Shoubra, Benha University, Cairo, Egypt.*
[2] *Faculty of Engineering (Shibin El kom), Menofia University.*
** Corresponding author*
*E-mail address: baselemad203@gmail.com, fatkader2@yahoo.com, elsherif.mohsen@yahoo.com , islam.ahmed@feng.bu.edu.eg*

**Abstract:** This paper presents an improved PI-controller for minimizing the ripple torque of switched reluctance motor (SRM) drives in electric vehicle applications. The motor speed is controlled by an optimized proportional-integral PI-controller in the outer loop, and the motor torque is controlled by an additional optimized PI-controller with a hysteresis controller in the inner loop. The controller gains are obtained based on a Harris Hawk's Optimization (HHO) Because of the nonlinear characteristics of the SRM. The objective function is to minimize the integration of the absolute error (IES). A 6/4 SRM is used to investigate the performance of the motor with the proposed controller using Matlab/Simulink toolbox. According to the simulation results, the suggested controller achieves to acceptable ripple torque and achieves the target speed.

## 1. Introduction

The development of electric vehicles (EVs) for urban transportation is primarily motivated by economic and environmental concerns[1]. For the EV designer, choosing the appropriate electric motor is of utmost importance. There are several different kinds of electrical machines such as switching reluctance motors (SRM), permanent magnet synchronous motors, and induction motors. The optimum choice of the motor is the result of a trade-off between the motor's power density, efficiency, cost, mass, volume, dependability, and maintenance. Therefore, the SRM is selected because of its great power density and good efficiency[2]- [5]. Because of these significant preferences, they are high-potential candidates for use in the electric vehicle industry. However, the SRM exhibits noticeable torque ripple and acoustic noises, preventing it from being used in high-performance applications[6]. Previous authors proposed two approaches to the torque ripple problem. The first method involves modifying the machine's design, such as changing winding configurations or optimizing its geometrical dimensions[7][10]. To a certain extent, this strategy may reduce the torque ripple and noise produced by the machine. But, once a machine has been manufactured, it is difficult to change its dimensions. The second approach relies on advanced control strategies[11]. To produce the maximum torque and reduced ripple torque of an SRM at a given speed, the combination of the motor and the power electronic converter should be fully controlled using Switched Reluctance Drive (SRD). SRD is composed of SRM, converter, and controller.

## 2. Modeling of the proposed system

As shown in Fig. (1), the proposed system consists of SRD applied to an EV. SRD consists of a speed controller, torque controller, and asymmetrical converter. The arrangement presented here assists us in minimizing torque ripple.

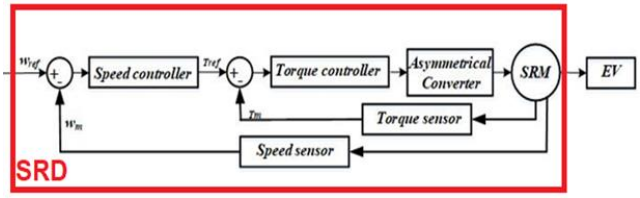


**Fig 1.** switched reluctance motor drive applied on electric vehicle

### 2.1 Modeling and design of an EV

As shown in Fig. (2), a moving car is subject to the Tractive force (FTR), aerodynamic force (FAD), gravitational force (Fgxt), and rolling force (Froll). The vehicle's propulsion system produces a tractive force (FTR). where it must outweigh the accelerating force (Fa) and the road load force (FRL) then, the vehicle forward at the appropriate speed[12][14].

$$F_{TR} = F_{RL} + F_a \tag{1}$$

The road forces consist of rolling resistance (Froll), aerodynamic drag (FAD), and gravitational force (Fgxt): $F_{RL} = F_{roll} + F_{AD} + F_{gxt}$

$$= C_o M_{veh} g + 0.5 \rho C_D A_f (V_{veh} + V_o)^2 + M_{veh} g \sin(\alpha) \tag{2}$$

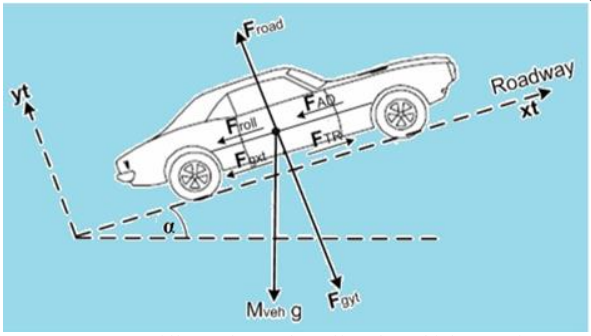


**Fig 2.** Different forces that affect the vehicle's motion

The load torque at the shaft of the wheel axle, Twh , can be expressed by:

$$T_{wh} = F_{RL}\, r_{wh} \tag{3}$$

Additionally, the motor axle's shaft is referred to as the load torque TL, which can be expressed by:

$$T_L = \frac{T_{wh}}{m} \tag{4}$$

The power rating of the electric motor drive in EV is entirely determined by vehicle acceleration performance requirements, motor characteristics, and transmission characteristics [15].

$$P_{mr} = \frac{K_m M_{veh}}{2t_a} V_f^2 + \frac{2}{3} C_0 M_{veh}\, g V_f + \frac{1}{5} \rho C_D A_f V_f^3 \tag{5}$$

The power rating of the motor drive can be estimated at the start of the design based on the acceleration performance, which is the time required to accelerate the vehicle from zero to a given speed. The first term in Eqn. (5) represents the power used to accelerate the vehicle mass, and the second and third terms represent the average power for overcoming the tire rolling resistance and aerodynamic drag.

Where: Mveh: the total mass of the vehicle in kg, g: gravitational acceleration constant (g =9.8 m/sec2), Co: coefficient of rolling resistance, ρ: air density (1.225 kg/m3), CD: aerodynamic drag coefficient (dimensionless and typically 0.2<CD<0.4), Af: equivalent frontal area of the vehicle in m2, V0: head-wind velocity (m/s), Vveh: vehicle speed (m/s), α: grade angle concerning the horizontal direction, rwh: radius of the wheel in meters, m: gear ratio of the gearbox.

### 2.2 Modeling of Switched Reluctance Motor

The difference in the magnetic reluctance of magnetic field lines between aligned and unaligned rotor positions is the basis of the SRM's operating concept. The rotor feels a force that pulls it to the aligned position when a stator coil is activated. The equivalent circuit for the SRM is consisting of resistance and inductance under some conditions. The parameters of the motor are shown in table (1). The equivalent circuit per phase for three phases of SRM is shown in Fig. (3). It consists of stator resistance per phase (Rs) and motor inductance (L)[16]-[19].

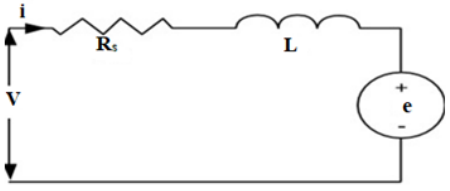


**Fig 3.** Single-phase equivalent circuit of SRM

The applied voltage to a phase is given as:

$$V = R_s i + \frac{d\lambda(\theta,i)}{dt} \tag{6}$$

Where λ is the flux linkage per phase which is given by:

$$\lambda = L(\theta,i)\, i \tag{7}$$

The value of L is dependent on the rotor position and the phase current.

The air gap power results in:

$$p_a = \frac{1}{2} i^2 \frac{dL(\theta,i)}{dt} = \frac{1}{2} i^2 \frac{dL(\theta,i)}{d\theta} \cdot \frac{d\theta}{dt} = \frac{1}{2} i^2 \frac{dL(\theta,i)}{d\theta} \omega_m \tag{8}$$

The air gap power is the product of the electromagnetic torque and rotor speed given by:

$$p_a = \omega_m T_e \tag{8}$$

From which the electromagnetic torque is obtained by:

$$T_e = \frac{1}{2} i^2 \frac{dL(\theta,i)}{d\theta} \tag{9}$$

**Table (1)** 6/4 SRM parameters.

| Motor parameters | Values |
|---|---|
| Rated Power | 60kw |
| Number of Phases | 3 |
| Number of Stator Poles 6 | 6 |
| Number of Rotor Poles | 4 |
| Aligned Phase Inductance | 23.6mH |
| Unaligned Phase Inductance | 0.67mH |
| Inertia | 0.05Kg.m |
| Stator Resistance | 0.05Ω |
| DC Voltage Supply | 240V |
| gear ratio (m) | 1.4575 |

At various motor terminal voltage and vehicle mass values, the steady-state operating points can be calculated. The intersection of the characteristics of the motor-developed torque and load torque at the various values of the motor terminal voltage and vehicle mass is the operational point, according to Fig. (4).

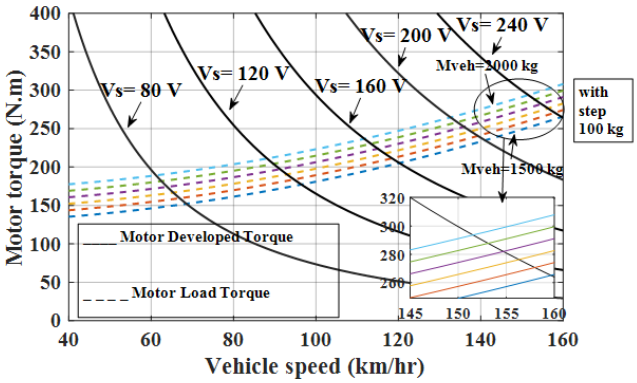


**Fig 4.** Motor-developed torque and load torque versus vehicle speed at different values of vehicle mass

### 2.3 Power electronics converter

A power electronics converter is required in SRM because the supply voltage is delivered to the phase terminal for a range of rotor positions (between the turn-on angle and turn-off angle). The motor's speed is determined by the amount of torque generated, which is determined by

the machine's flux linkage profile. The SRM is fed by a three-phase asymmetric converter as shown in fig. (5) which allows for independent control of the phases[10],[20][21].

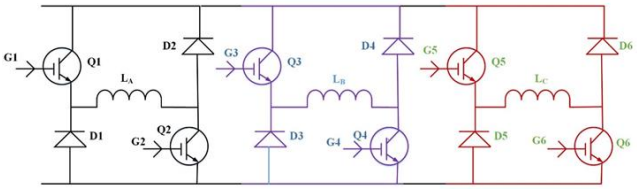


**Fig 5.** Three-phase asymmetric bridge converter

## 3. The Proposed controller of the System

The SRM has two control modes: voltage control and current control. The desired current is achieved in the current control mode by modulating the phase voltage. The PWM signal's duty cycle modulates the phase voltage based on the phase current difference between the set and actual values.

The voltage applied to the phases is kept constant in voltage control mode for a fixed dwell period. The control method varies with the rotational speed. Because current regulation at each phase is impossible, voltage control is used. The voltage applied to the motor phases is constant during the entire sampling period of the torque speed-control loop in voltage control.

A torque speed controller directly regulates the voltage provided to the phase. Speed error processing is done by the speed controller (the difference between the desired speed and the actual speed). This error demonstrates the reference torque for the torque controller, whose output is presumably processed by a hysteresis controller with a torque window of Δt. As depicted in Fig. (6) (a), the switches T1 and T2 are simultaneously activated when the torque error is within the limit. When the torque error exceeds Δt, the switches T1 and T2 are turned off simultaneously. Due to its straightforward concept and application, the hysteresis current controller is taken into consideration in this article. As indicated in Fig. (6) (b), diodes D1 and D2 then take control of the current and finish the passage via the dc source.

Based on the torque tracking error, these solutions mostly use PI controllers to determine the duty cycle for a hysteresis controller. The torque signal and the speed signal are the system's two feedback signals. That is double closed-loop PI control: torque PI inner loop control and speed PI outer loop control. The proposed control structure is shown in Fig. (1). The maximization of the torque is achieved by Harris Hawk's optimization (HHO).

The optimal values of the PI-controller gains are to minimize the Integral Squared Error (ISE) of the torque, and speed ripples computed from the inner and outer loop can be considered as an objective for both conventional and AI tuning techniques. Accordingly, the objective function (ISE) is given by:

$$ISE = \int_0^{\infty} \left|(W_{ref} - W_m)\right| dt + \int_0^{\infty} \left|(T_{ref} - T_m)\right| dt \qquad (10)$$

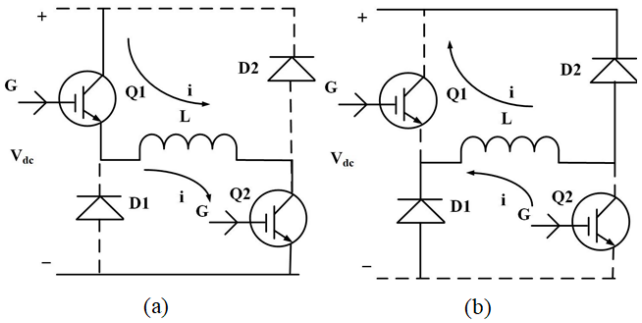


**Fig 6.** Modes of operation of one phase of bridge converter: (a) Excitation mode (b) de-energization mode

The main source of inspiration for HHO is the natural cooperative behavior and chasing style of Harris' hawks known as surprise pounce. Several hawks work together to pounce on prey from different directions in an attempt to catch it off guard. Harris hawks can exhibit a variety of chasing patterns based on the dynamic nature of scenarios and the prey's escaping patterns. To develop an optimization algorithm, this work mathematically mimics such dynamic patterns and behaviors[22][23].

## 4. Simulation Results and Discussion

The relationship between the instantaneous phase flux linkage and the instantaneous phase current over the entire range of rotor displacement is represented by the flux linkage profile (the magnetization curve). Fig. (7) depicts the flux linkage's change concerning the current for various motor rotor positions.

The measurements of flux and torque data are repeated numerous times depending on the necessary resolution of the rotor position to obtain the complete motor characteristics. In Fig. (8) (a), (b), and (c) the flux and torque characteristics are displayed. Both the flux and torque measurements are highly nonlinear functions of the current and rotor position, as seen in the figures. To represent the machine, these data are used as look-up tables.

Between a minimum and a maximum value, the unsaturated inductance fluctuates. When a rotor pole is sandwiched between two stator poles, the value is at its lowest. When a stator pole and a rotor pole are lined up, the maximum is reached. The block linearly approximates the unsaturated inductance as a function of the rotor angle in the region between these locations. The unsaturated inductance as a rotor pole crosses a stator pole is depicted in Fig. (9).

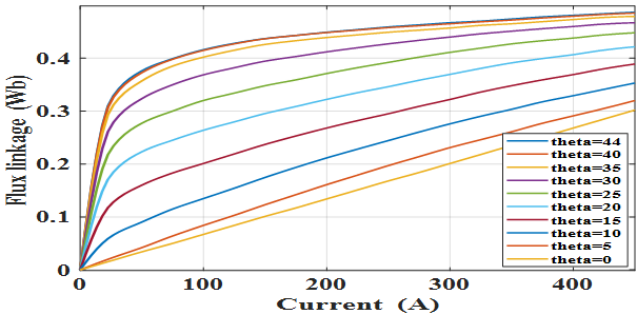


**Fig 7.** Magnetization characteristics for 3-ph 6/4 SRM

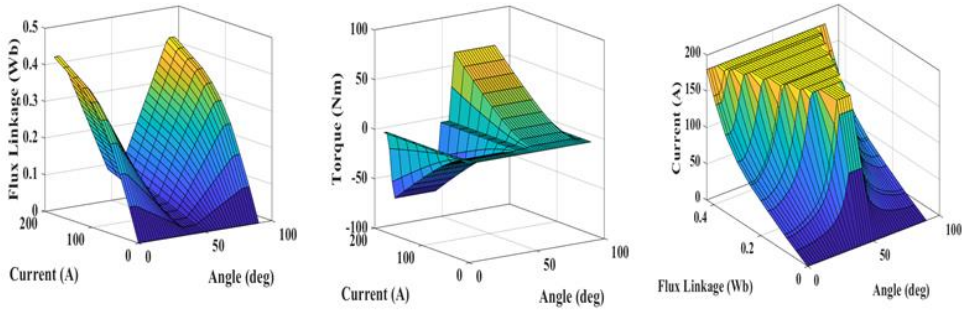


**(a)** **(b)** **(c)**

**Figure 8. (a)** The phase flux linkage versus electrical angle characteristics at different motor currents (0 to 200A), **(b)** The electromagnetic torque versus electrical angle characteristics at different motor currents, **(c)** The phase current versus electrical angle characteristics at different flux Linkage

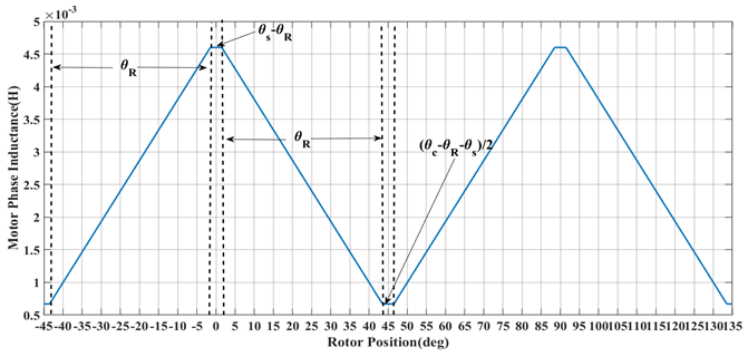


**Figure 9.** Motor phase inductance versus rotor position, θR : Angle subtended by each rotor pole parameter, θS : Angle subtended by each stator pole parameter ,θC : corresponds to the angle subtended by this full cycle.

### Case1: Rotor position at different turn-on angles and step load torque.

To accommodate the application of an electric vehicle with a certain number of passengers, the motor load torque should be variable. It goes from zero to 50, then 100, then 200, each load being applied for two seconds. Apply the control approach after characterizing the motor with a different switching angle to extract the maximum torque of the motor at a specified switching angle.

Fig. (10) shows the motor characteristic curves at a turn-on angle of 35º: motor speed, phase current, developed motor torque, and the average power. the motor torque and current ripples are at their highest value when the load torque is at 200 (N.m). where is changed from 70:260 (N.m) and 0:110 (A). Also, the motor speed drops to 624:520 (rad/sec) but the motor's average power rises to 50:70 (kW).

Fig. (11) explain the motor characteristic curves at a turn-on angle of 40º: motor speed, phase current, developed motor torque, and the average power. Infer from this that the highest value of torque and current ripples, which occurred when the load torque at 200 (N.m), runs from 80:350 (N.m) and 0:120 (A.) Also, the motor speed drops to 416:520 (rad/sec), but the average power rises to 40:55 (kW).

Fig. (12) shows the motor characteristic curves at a turn-on angle of 45º: motor speed, phase current, developed motor tor,que and the average power. The maximum torque and current ripples range from 75:270 (N.m) and 0:115 (A). Also, the speed decreases to 312:374 (rad/sec) but the average power increases to 40:65 (KW) and this occurred when the load on the motor is at 200 (N.m). In this case, Table 2 summarizes the remaining results.

Table 2 provides a summary of the simulation results for the motor's properties at various switching angles. It is evident that the torque ripple in the motor increases along with the load on the motor. A control strategy to reduce ripple must be utilized to take advantage of the highest motor torque, which is at a turn-on angle of 40º and a load torque of 200 (N.m). This torque is accompanied by the highest ripple value of 80:350 N.m.

### Case 2: Torque and Speed Control

Following the application of the control method, several outcomes that represent the speed and torque will be displayed in this sector. Using the information provided above, we were able to calculate the switching angle that was employed. We were also able to apply the HHO algorithm to extract the values for the optimized pi controller.

To explore the effectiveness of the proposed technique, Both the conventional and the optimized PI controller were applied to the motor. The results of applying the optimized PI controller to the SRM were compared to those obtained by the application of the conventional PI controller. The conventional PI controller gains are obtained from trial and error.

The comparison will yield results in one of three scenarios: either the reference speed that must be reached must be constant (2000 rpm) while the load torque must be variable as shown in Fig. (13) (a), or the reference speed

that must be reached must be variable as shown in Fig. (13) (b) while the load torque must be fixed (50 N.m), or both the load torque and the reference speed must be variable. to demonstrate the ideal setup for them.

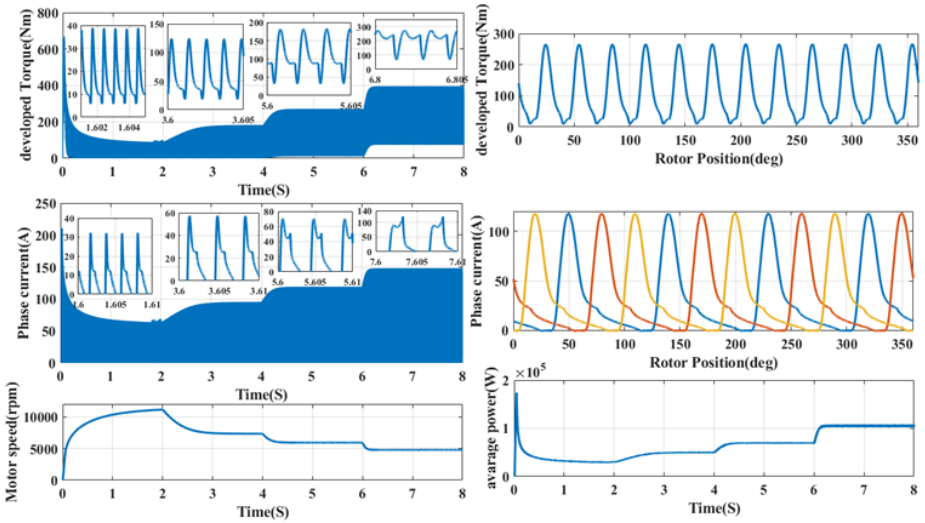


**Fig 10.** motor Characteristics at a turn-on angle of 35º and turn-off angle of 75º.

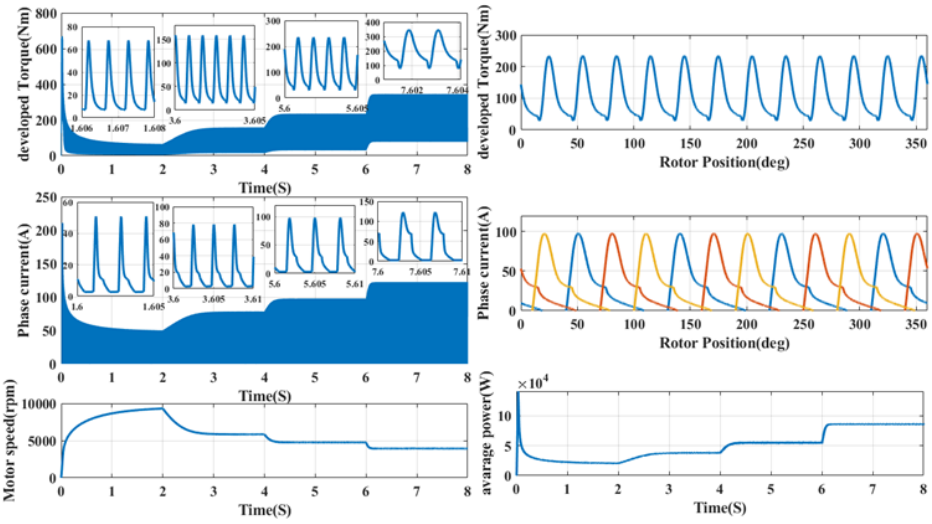


**Fig 11.** motor Characteristics at a turn-on angle of 40º and a turn-off angle of 75º.

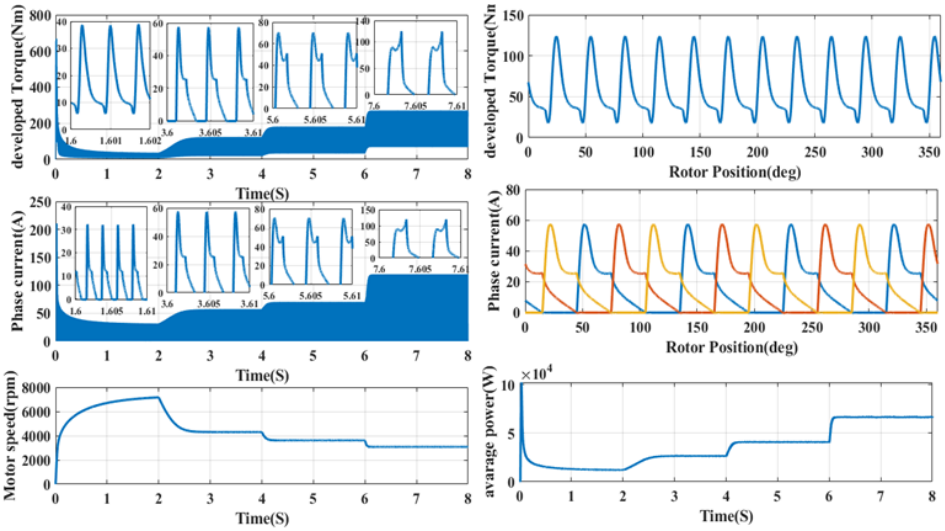


**Fig 12**. motor Characteristics at a turn-on angle of 45º and a turn-off angle of 75º.

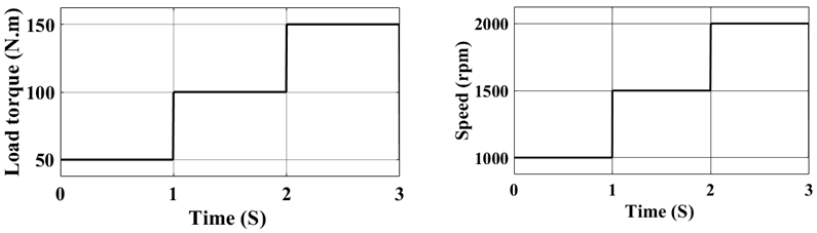


(a) (b)

**Figure 13. (a)** different load torque**, (b)** variable reference speed

**Table (2)** summarized the simulation results.

| $\theta_{on}$ & $\theta_{off}$ | 35º & 75º | | | | 40º & 75º | | | | 45º & 75º | | | |
|---|---|---|---|---|---|---|---|---|---|---|---|---|
| **Load torque (N.m)** | 0 | 50 | 100 | 200 | 0 | 50 | 100 | 200 | 0 | 50 | 100 | 200 |
| **Ripple current (A)** | 0:30 | 0:60 | 0:70 | 0:110 | 0:50 | 0:80 | 0:100 | 0:120 | 0:30 | 0:55 | 0:70 | 0:115 |
| **Ripple torque (N.m)** | 10:40 | 20:120 | 30:180 | 70:260 | 10:56 | 12:155 | 30:230 | 80:350 | 5:40 | 20:120 | 35:180 | 75:270 |
| **Motor speed (rad/sec)** | 0:1144 | 1144:760 | 760:624 | 624:520 | 0:9670 | 9670:624 | 624:520 | 520:416 | 0:728 | 728:447 | 447:374 | 374:312 |
| **Motor average power (kW)** | 170:30 | 30:50 | 50:70 | 70:107 | 140:20 | 20:40 | 40:55 | 55:90 | 102:12 | 12:27 | 27:40 | 40:65 |

Fig. (14) shows the torque-speed response of the SRM with the conventional PI and the optimized PI controller respectively in cases of fixed load torque at 50 (N.m) and variable reference speed. It can be seen from the Figure that optimized PI provides better performance by reducing the torque ripple to 4% better than conventional PI which only provided reducing in torque ripple by 9%. Also, in tracking speed optimized PI only need 0.02 sec settling time better than conventional which needs 0.1 sec. Table 3 summarizes the remaining results.

In the scenarios of varying load torque and constant reference speed at 2000 (rpm), the torque-speed response of the SRM with the traditional PI and the improved PI controller, respectively, is shown in Fig. (15). The Figure shows that, compared to traditional PI, which could only reduce torque ripple by 12%, optimized PI offers greater performance by cutting torque ripple to 4%. Additionally, tracking speed optimized PI requires less settling time than conventional, only 0.04 sec as opposed to conventional 0.15 sec. The remaining results are summarized in Table 3.

Figure (16) depicts the torque-speed response of the SRM with the conventional PI controller and the optimized PI controller in the presence of variable load torque and variable reference speed. The Figure shows that optimized PI outperforms conventional PI by reducing torque ripple by 5%. Furthermore, tracking speed-optimized PI requires only 0.02 sec settling time, as opposed to conventional, which requires 0.1 sec. Table 3 summarizes the remaining results.

The ripple torque is given by:

$$\text{RippleTorque} = \frac{T_{\max} - T_{\min}}{T_{avg}} \quad (11)$$

Where: Tmax : the maximum torque ripple, Tmin: the minimum torque ripple and Tavg: the average torque ripple.

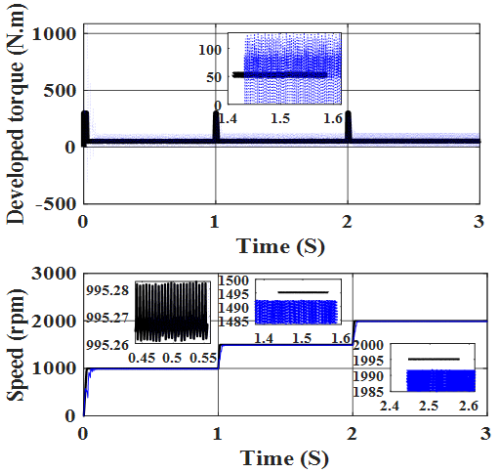


**Fig 14.** SRM performance with Constant load torque and fluctuating reference speed

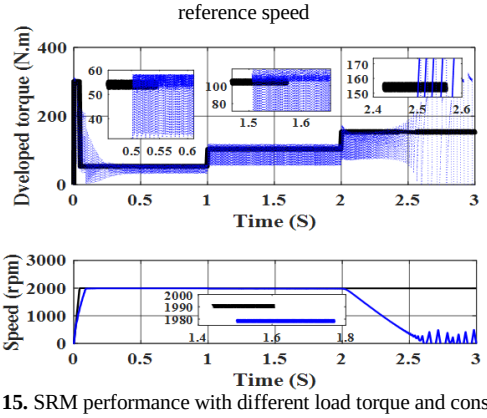


**Fig 15.** SRM performance with different load torque and constant reference speed

The simulation result of these cases is summarized in table 3.

As seen from the table, all results indicate that the optimized PI controller has also less overshoot and ripple than the result obtained by the conventional PI controller. The optimized PI gives reduced rise time as well as small overshoot with or without load and also different reference speeds. Hence, the optimized PI controller is capable of providing sufficient torque-speed tracking compared with the conventional PI controller.

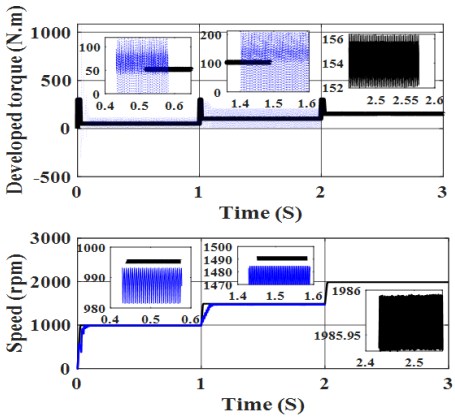


**Fig 16.** SRM performance with different load torque and fluctuating reference speed

**Table (3)** summarized the simulation results.

| | Constant load torque and fluctuating reference speed | | different load torque and constant reference speed | | different load torque and fluctuating reference speed | |
|---|---|---|---|---|---|---|
| | **optimized** | **conventional** | **Optimized** | **conventional** | **optimized** | **conventional** |
| **Ripple torque** | 4% | 9% | 4% | 12% | 5% | 18% |
| **Settling time** | 0.02 | 0.1 | 0.04 | 0.15 | 0.02 | 0.2 |
| **Steady-state error** | 0.5% | 1.5% | 0.25% | 1.2% | 0.5% | 1.5% |

## Conclusions

This paper presents a PI controller-based torque-speed control approach for 3-phase 6/4 SRM. According to the results, the improved PI controller operates more effectively than a conventional PI controller. This can reduce steady-state error by 75%, torque ripple by 50%, and settling time by 80%. For instance, in the case of the highest load torque of 200 (N.m), the turn-on angle of 40º optimized PI controller gives 4% while the conventional PI controller gives 9% torque ripple, settling time in the case of optimized PI controller 0.02 sec while conventional PI controller gives 0.1 sec, and steady-state error in optimized PI controller 0.5% while conventional PI controller gives 1.5%.

### REFERENCES


[1] Rajashekara, Kaushik. "Present status and future trends in electric vehicle propulsion technologies." IEEE journal of emerging and selected topics in power electronics 1.1 (2013): 3-10.

[2] Aliasand, Arun Eldho, and F. T. Josh. "Selection of motor foran electric vehicle: A review." Materials Today: Proceedings 24 (2020): 1804-1815.

[3] De Santiago, Juan, et al. "Electrical motor drivelines in commercial all-electric vehicles: A review." IEEE Transactions on vehicular technology 61.2 (2011): 475-484.

[4] Xue, X. D., Ka Wai Eric Cheng, and N. C. Cheung. "Selection of electric motor drives for electric vehicles." 2008 Australasian Universities power engineering conference. IEEE, 2008.

[5] Andrada, Pere, et al. "Switched reluctance drives for electric vehicle applications." RE & PQJ 1.1 (2003): 311-317.

[6] Seshadri, Arjun, and Natesan Chokkalingam Lenin. "Review based on losses, torque ripple, vibration and noise in switched reluctance motor." IET Electric Power Applications 14.8 (2020): 1311-1326.

[7] Bhuvaneswari, S., et al. "Super Core Magnetic Material based Switched Reluctance Motor for Electric Vehicle Applications." IOP Conference Series: Materials Science and Engineering. Vol. 1084. No. 1. IOP Publishing, 2021.

[8] Wang, Ruihao, et al. "A New Optimization Method for Pole-arc Parameters of Variable-gap Two-phase Switched Reluctance Motor." Journal of Physics: Conference Series. Vol. 2218. No. 1. IOP Publishing, 2022.

[9] Dmitrievskii, Vladimir, Vladimir Prakht, and Vadim Kazakbaev. "Novel rotor design for high-speed flux reversal motor." Energy Reports 6 (2020): 1544-1549.

[10] Siadatan, Alireza, Mohamadmeisam Roohisankestani, and Saeid Farhangian. "Design and Simulation of a new Switched Reluctance Motor with changes in the shape of stator and rotor in order to reduce torque ripple and comparison with the conventional motor." 2018 International Symposium on Power Electronics, Electrical Drives, Automation and Motion (SPEEDAM). IEEE, 2018.

[11] Abdel-Fadil, Reyad, Fahad Al-Amyal, and László Számel. "Torque ripples minimization strategies of switched reluctance motor-A review." 2019 International IEEE Conference and Workshop in Óbuda on Electrical and Power Engineering (CANDO-EPE). IEEE, 2019.

[12] Vempalli, Sai Krishna, et al. "Electric vehicle designing, modelling and simulation." 2018 4th International Conference for Convergence in Technology (I2CT). IEEE, 2018.

[13] Ni, Liqin, Dean Patterson, and Jerry L. Hudgins. "Preliminary design, simulation and modeling of a series hybrid commuter vehicle with a minimal IC engine." 2007 IEEE Vehicle Power and Propulsion Conference. IEEE, 2007.

[14] Choi, Gilsu, and T. M. Jahns. "Design of electric machines for electric vehicles based on driving schedules." 2013 International Electric Machines & Drives Conference. IEEE, 2013.

[15] Deepak, M., G. Janaki, and C. Bharatiraja. "Design and Development of High-Performance 3kW Electric Vehicle Grade Switched Reluctance Motor." ECS Transactions 107.1 (2022): 1897.

[16] Krishnan, Ramu. Switched reluctance motor drives: modeling, simulation, analysis, design, and applications. CRC press, 2017.

[17] Sun, Baojiang, and Jianhui Wang. "Model Construction and Simulation of Switched Reluctance Motor Based on MATLAB/S Function." Journal of Physics: Conference Series. Vol. 1813. No. 1. IOP Publishing, 2021.

[18] Chaple, Megha, and Sanjay B. Bodkhe. "The simulation and mathematical modeling of switched reluctance motor based on phase winding inductance." 2017 International Conference on Energy, Communication, Data Analytics and Soft Computing (ICECDS). IEEE, 2017.

[19] Ma, Qingqing, et al. "A new modeling method for S-MCSRM driven by three-phase full bridge converter." Compel: The International Journal for Computation and Mathematics in Electrical and Electronic Engineering (2014).

[20] Bae, Han-Kyung, et al. "A linear switched reluctance motor: converter and control." IEEE Transactions on Industry Applications 36.5 (2000): 1351-1359.

[21] Deepak, M., G. Janaki, and C. Bharatiraja. "Power electronic converter topologies for switched reluctance motor towards torque ripple analysis." Materials Today: Proceedings 52 (2022): 1657-1665.

[22] Bao, Xiaoli, Heming Jia, and Chunbo Lang. "A novel hybrid harris hawks optimization for color image multilevel thresholding segmentation." Ieee Access 7 (2019): 76529-76546.

[23] Heidari, Ali Asghar, et al. "Harris hawks optimization: Algorithm and applications." Future generation computer systems 97 (2019): 849-872.